Improvement of Runoff Simulation of the Amur River

Takeo ONISHI[1*], Muneoki YOH[2], Seiya NAGAO[3] and Hideaki SHIBATA[4]

[1]*Faculty of Applied Biological Sciences, Gifu University, Japan*
1-1 Yanagido, Gifu 501-1193, Japan
[2]*Tokyo University of Agriculture and Technology, Japan*
[3]*Low Level Radioactivity Laboratory, Kanazawa University, Japan*
[4]*Field Science Center for Northern Biosphere, Hokkaido University, Japan*
**e-mail: takeon@gifu-u.ac.jp*

Abstract

Recent studies show that dissolved iron is a factor essential to the biological productivity of the Sea of Okhotsk. It is also highly probable that wetlands in the Amur River basin play an important role in providing dissolved iron to the Sea of Okhotsk. During the last century, large areas of wetlands within the Amur River catchment have been cultivated, which, in turn, may have had a great impact on the production of dissolved iron. To assess the impact of this conversion of land cover on the production of dissolved iron – and thereby primary production in the Sea of Okhotsk – we have been constructed a numerical model to simulate dissolved iron production and transport in the Amur River.

Though the accuracy of hydrological models heavily depends upon the precipitation input, there has been no observation-based gridded precipitation dataset covering a continental-scale region with high spatio-temporal resolution. Recently, however, datasets such as APHRODITE have been released. Thus, in this article we evaluate how hydrological simulation results may be improved by these datasets. By comparing the results from the APHRODITE precipitation dataset with those from the NCEP2 precipitation dataset, we show that the precipitation amount from NCEP2 around the Amur River basin is overestimated. Moreover, the closeness of the fit evaluated by the Nash-Sutcliffe criteria indicates that the results from APHRODITE are significantly better than those from NCEP2. The results indicate that the precipitation of the APHRODITE dataset for the Amur River basin has good accuracy.

Key words: Amur River, APHRODITE, dissolved iron, Sea of Okhotsk, wetland

1. Introduction

The Amur River, which rises in Mongolia, is one of the world's largest rivers, comprising a long stretch of the boundary between China and Russia. The catchment area of the river is about 2,100,000 km^2, the ninth largest river catchment in the world, and the total length of the river is about 4,400 km. Therefore, a huge quantity of fresh water is supplied by the Amur River to the Sea of Okhotsk (Ogi *et al*., 2001).

The Sea of Okhotsk is one of the most biologically productive regions of the world; and it supports a highly productive commercial fishery. Martin and Fitzwater (1988) found that phytoplankton growth depends on iron abundance as a limiting factor in the Northeast Pacific Ocean. Recent studies show that dissolved iron plays an important role in maintaining the biological productivity of the Sea of Okhotsk (Boyd *et al*., 2004), and it is highly possible that one of the most important sources of dissolved iron is fresh water from the Amur River (Ducklow *et al*., 2003).

Iron is an essential nutrient not only for the biological productivity of the Sea of Okhotsk but also for most biota. However, the production and transportation of dissolved iron through the terrestrial part of this ecosystem is not well understood. A complicating factor, especially in the last few decades, has been that extensive regions of agricultural land have been developed through drainage improvements to wetlands (Wang *et al*., 2004).

To investigate the mechanism of dissolved iron production and to evaluate the effect of land cover change, we have developed a simple hydrological model incorporating dissolved iron production to simulate discharge and the distribution of dissolved iron in the Amur River basin. Though the accuracy of hydrological models heavily depends upon the precipitation input, there has been no global-scale daily gridded precipitation data set based on observational data. Thus, global reanalysis data sets such as National Centers for Environmental Predictions (NCEP) / Department of Energy (DOE) Atmospheric Model Intercomparison Project (AMIP)-II Reanalysis (Kanamitsu *et al*., 2002) and European Centre

for Medium-range Weather Forecasts (ECMWF) reanalysis (ERA40) (Kållberg *et al.*, 2004) <http://www.ecmwf. int/research/era/> have been commonly used especially for continental scale hydrological simulations. Since the main objective of constructing reanalysis data sets is producing a consistent global analysis of the state of the atmosphere over an extended period of time, precipitation figures in reanalysis data sets are entirely computationally reproduced fields through 4-dimensional data assimilating processes utilizing historic archives of observations.

In contrast to this, several gridded highly-resolved climate data sets such as the Asian Precipitation - Highly-Resolved Observational Data Integration Towards Evaluation of Water Resources (APHRODITE's Water Resources) (Yatagai *et al.*, 2009) or H08 (Hirabayashi *et al.*, 2008) have recently been released. Since these data sets are basically based on observational data, and have high spatio-temporal resolution, these data sets should have a potential to improve the accuracy of hydrological simulation results. Thus, in this paper, we have attempted to compare the result of our hydrological model with different precipitation data sets. In the rest of paper, we will refer to those datasets as NCEP2, ERA40, APHRODITE, and H08 for brevity.

2. Site Description

The study site is shown in Fig. 1. The amount of annual fresh water supplied to the Sea of Okhotsk by the river is about 300 km^3. The average annual precipitation ranges from 300 mm in the west to more than 700 mm in the east. The mean annual temperature also varies from –7ºC in the north to 6ºC in the south.

Figure 2 shows the spatial pattern of land use and land cover (LULC) types of the basin. LULC types of the basin are categorized into 19 types. The most dominant LULC type is forest consisting of mixed forest, deciduous forest, coniferous forest, shrubs, and sparse growth. Next, agricultural lands (dryland and paddy fields) occupy a major part of the land cover. Most of the drylands are located on the China side and occupy about 40% of the area of the Songhua River basin. The main crops are maize, soybeans, wheat and rice (Park *et al.*, 2001). The rest of the basin mainly consists of grasslands and wetlands. Grasslands and wetlands occupy 12.2% and 6.9% of the basin, respectively. While most of the grasslands cover the upper reaches of the basin, wetlands are mainly located along the main course of the lower reach (from the river mouth to Khabarovsk) of the Amur River. These four different land cover types, *i.e.*, forests, agricultural lands, grasslands, and wetlands cover more than 96% of the basin.

3. Materials and Methods

3.1 Model structure

We first divided the whole river basin into 0.5°×0.5°grids. We considered each grid as one watershed as is usual in LSM. We then routed the discharge from each basin along the river network. A schematic diagram of the model for each divided basin is shown in Fig. 3. Each grid was again subdivided into 1,000 m × 1,000 m grids and the discharge from each

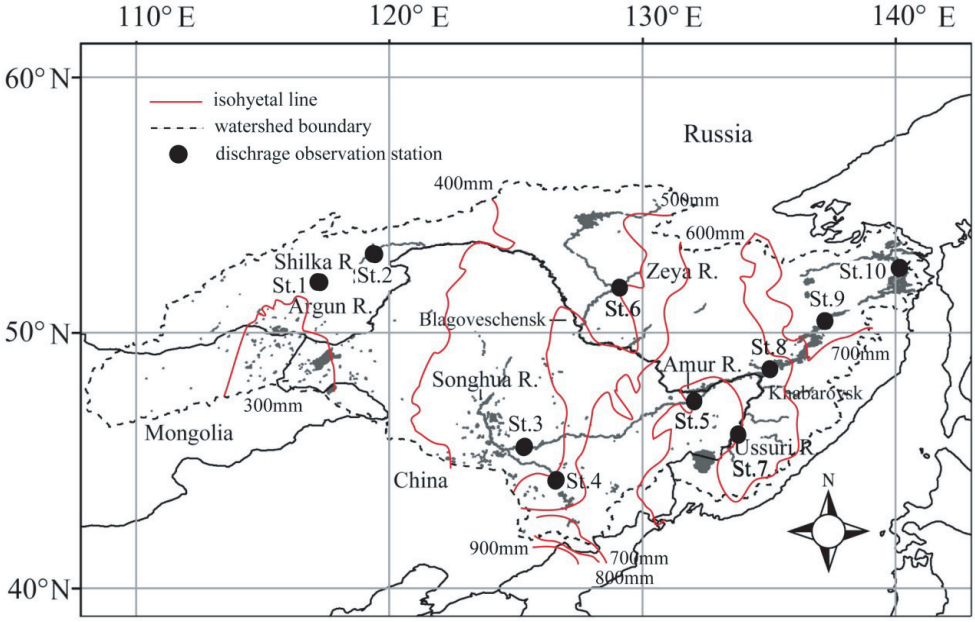

Fig. 1 Outline and annual precipitation pattern of the Amur River Basin. Names of main tributaries are shown. Black circles indicate locations of observation stations the data of which are used in this paper. For precipitation, a figure in Simonov and Dahmer (2008) was modified.
Original data sources: *Atlas of the People's Republic of China*, Foreign Language Press, Beijing, 1989; Carmen Revenga, Siobhan Murray, Janet Abramovitz, and Allen Hammond, *Watersheds of the World: Ecological values and vulnerability*, World Resources Institute, Washington, 1998; Gerhard Heilig, *Chinafood: Can China Feed Itself?* (CD-ROM), IIASA, Laxenburg, 1999.

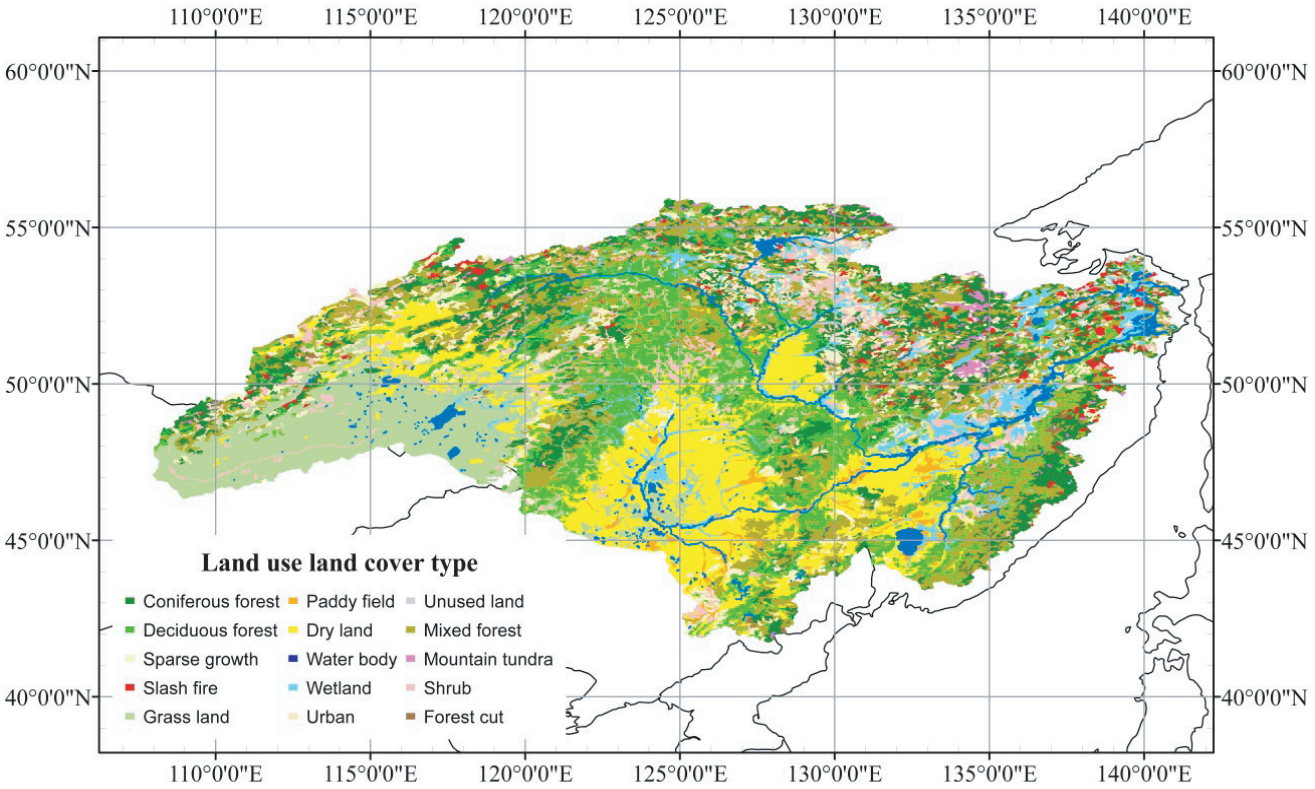

Fig. 2 Land use / land cover type of the Amur River Basin in 2000 (Yermoshin *et al.*, 2007). The map was constructed by combined utilization of vegetation maps of China, Mongolia and Russia and satellite imageries.

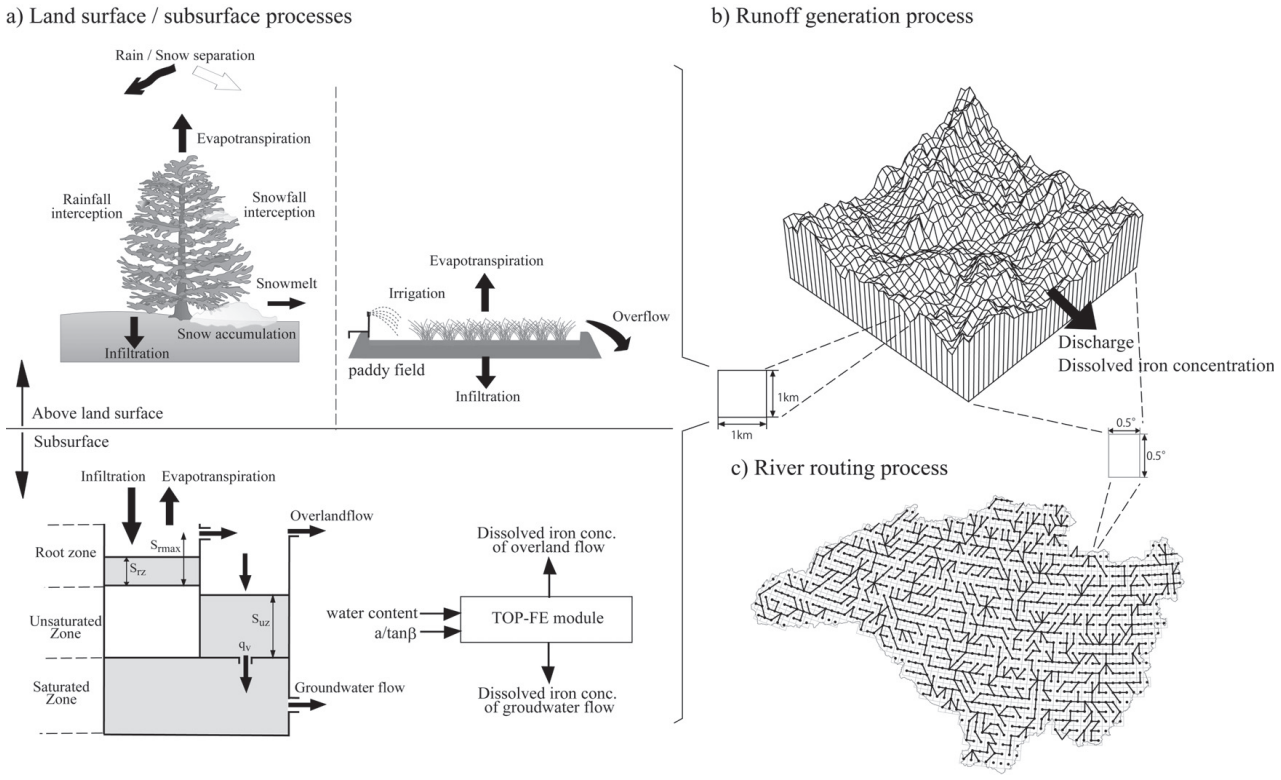

Fig. 3 Schematic diagram of the hydrological model.

Table1 List of external parameters of the model. Parameters are classified into four categories. Phenological parameters and soil physical parameters are prescribed according to land use/land cover type and soil type prescribed with horizontal distribution. The number of calibration parameters is also kept to a minimum as much as possible.

Symbol	Description	Unit	Resolution	Value	Source
prescribed with horizontal distribution					
	land use / land cover type	–	1000m		Yermoshin *et al*. (2007)
	soil type	–	1°		ISLSCP II[b]
	elevation	m	1000m		SRTM-3
a/tanβ	topographic index	m	1000m		SRTM-3
prescribed with land use / land cover type					
LAI	leaf area index	m^2/m^2	1000m		Li *et al*. (2003), Liua (2005), Scurlock (2001)
g_s	surface conductance	m/s	1000m		Kondo (1994)
g_a	aerodynamic conductance	m/s	1000m		Kondo (1994)
h	canopy height	m	1000m		Yermoshin *et al*. (2007)
S_B	upper limit of canopy storage of snow	mm	1000m		
k	fitting parameter for canopy storage curve of snow	1/mm	1000m		Lundberg and Halldin (2001)
P_0	fitting parameter for canopy storage curve of snow	mm	1000m		
prescirbed with soil type					
T_0	saturated hydraulic conductivity	m/s	1°		ISLSCP II[˘]
SR_{max}	maximum root zone deficit	m	1°	–	ISLSCP II[˘]
prescirbed as constant					
T_s	threshold temperature for 100%snow	K	–	0.0	DeWalle and Rango (2008)
T_r	threshold temperature for 100%rain	K	–	4.5	DeWalle and Rango (2008)
F	degree-day factor for snow melt	cm/K/day	–	0.5	Hock (2003)
T_F	threshold temperature for snow melt	K	–	0.0	DeWalle and Rango (2008)
PD_c	upper limit of ponding depth of paddy fields	m	–	0.1	–
rm	river meandering ratio	–	–	1.4	Oki and Sud (1998)
calibration parameter (prescribed as constant)					
szm	scaling parameter for runoff	m	–	–	–
t_d	time constant for recharge to the saturated zone	m/h	–	–	–
chv	river routing velocity in one grid	m/s	–	–	–
rv	river routing velocity in river runoff routing	m/s	–	–	–
SD_c	dissolved iron production threshold	day	–	–	–

a: Product of Amur-Okhotsk project
b: Hall, Forrest G., G. Collatz, S. Los, E. Brown de Colstoun, D. Landis, eds. ISLSCP Initiative II. NASA. DVD/CD-ROM. NASA, 2005.

watershed was calculated using a runoff module. The model consists of two parts, in one of which parameters are determined and runoff is calculated (TOP-RUNOFF), and in the other, the dissolved iron production process is calculated (TOP-FE). The calculation time step can be set at any length, so we executed all calculations at a time step of one day in the analysis. Detailed explanations of the calculation algorithm for each process will be given below in sections 3.1.1 to 3.1.5. All external and input parameters needed to run the model are summarized in Table 1.

3.1.1 Precipitation / Interception / Snow melt

Depending on the daily mean air temperature, the precipitation amount is divided into rainfall or snowfall in accordance with the following equations.

$$\begin{aligned} &P_r = P, T_a \geq T_r \\ &P_r = P\frac{T_a - T_s}{T_r - T_s}, P_s = P - P_r, T_s < T_a < T_r \\ &P_r = 0, P_s = P, T_a \leq T_s \end{aligned} \tag{1}$$

Here, P_r is rainfall amount [mm day^{-1}], P_s is snowfall amount in equivalent water [mm day^{-1}], T_r and T_s are upper and lower temperature threshold values, respectively, of the rainfall/snowfall division [K], and T_a is the daily mean air temperature [K]. T_r and T_s are prescribed constant parameters fixed as 4.5 and 0.0 respectively (Hock, 2003; DeWalle & Rango, 2008).

The interception ratio of land vegetation is prescribed as a constant value according to the LULC type, except for foresst. For forests (coniferous forests, deciduous forests, and mixed forests), the rainfall interception rate and snowfall interception rate are separately estimated by the following equations (Lundberg & Halldin, 2001; Toba & Ohta, 2005).

$$I_r = P_{rg} exp(-0.04 P_{rg}), P_{rg} \leq 40 \tag{2}$$

$$I_r = 0.2 P_{rg}, P_{rg} > 40$$

$$I_s = \frac{S_B}{1 + exp\left(-k(P_{sg} - P_0)\right)} \tag{3}$$

Here, I_r is the interception loss of rainfall [mm], P_{rg} is the cumulative rainfall in one event, I_s is the interception loss of snow in water equivalent [mm], P_{sg} is the cumulative snow fall, S_B is the upper limit of canopy storage [mm], k is a fitting parameter [mm^{-1}], and P_0 is another fitting parameter [mm]. According to Lundberg and Halldin (2001), S_B, k, and P_0 are given as 4.13, 0.72, and 2.58 respectively.

The snow pack accumulation amount was calculated by simply summing up daily snowfall amounts. In the snow pack melting process, our model adopted the simplest form of the degree-day method as shown in the next equation

$$M = F\max(0, T_a - T_F) \tag{4}$$

Here, M is the melt rate as a water equivalent per unit area [cm day^{-1}], F is the degree-day factor [cm K^{-1} day^{-1}], T_a is the mean daily air temperature [K], and T_F is the threshold temperature [K]. F and T_F are prescribed constant parameters fixed at 0.5 and 0.0.

3.1.2 Evapotranspiration

The actual evapotranspiration rate was estimated by the Penman-Monteith (Monteith, 1965) equation as shown in the following equation:

$$\lambda_v E = \frac{\Delta(R_n + L - G) + \rho_a c_p (e_s - e_a) g_a}{\Delta + \gamma\left(1 + g_a / g_s\right)} \tag{5}$$

Here, E is the evapotranspiration rate [mm d^{-1}], R_n is net shortwave radiation [W m^{-2}], L is net longwave radiation [W m^{-2}], G is soil heat flux [W m^{-2}], ρ_a is the density of dry air [kg m^{-3}], c_p is the specific heat capacity of air [J kg^{-1} K^{-1}], e_s is the saturated vapor pressure at that air temperature [Pa], e_a is the vapor pressure of air [Pa], λ_v is the latent heat of water vaporization [J kg^{-1}], Δ is the rate of change of the saturation vapor pressure with air temperature [Pa K^{-1}], γ is the psychrometric constant [Pa K^{-1}], g_a is aerodynamic conductance [m s^{-1}], and g_s is surface conductance [m s^{-1}]; with λ_v set as 2.5 x 10^6 [J kg^{-1}], and γ set as 0.66.

To realize the simplest model and to reduce the computational burden as much as possible, heat conduction of soil is not considered in the present version of the model, *i.e.*, G is assumed to be 0. Since no calculation algorithm of upward long wave radiation is incorporated in the model, net long wave radiation is given as forcing data using NCEP2 data. For the same reason, net short wave radiation is also given as forcing data using NCEP2 data. This means that the separation between latent heat flux and sensible heat flux is calculated by equation (5) under the assumption that the net heat flux to the ground surface is appropriately given. Thus, aerodynamic conductance and surface conductance are unknown parameters in equation (5). Aerodynamic conductance is determined by the following equation:

$$r_a = \frac{\ln\left[\frac{z_w - d}{z_0}\right]\ln\left[\frac{z_h - d}{z_T}\right]}{k^2 u} \tag{6}$$

Here, z_w is the wind measurement height [m], z_h is the specific humidity measurement height [m], d is zero plane displacement [m], z_0 is surface roughness for wind [-], z_T is surface roughness for specific humidity [-], k is the von Karman constant = 0.4 [-], and u is the wind velocity [m s^{-1}]. Since analytical solutions of zero plane displacement, surface roughness for wind and surface roughness for specific humidity are obtained under the assumption of vertically homogeneous vegetation (Watanabe & Kondoh, 1990; Watanabe, 1994), we utilized these formulas to calculate the aerodynamic conductance of each LULC type.

On the other hand, surface conductance is considered to be a changing parameter with respect to soil water content, and determined by the next equation:

$$g_S = g_{S\max}\frac{S_{rz}}{SR_{\max}} \tag{7}$$

Here, $g_{s\max}$ is maximum surface conductance [m s^{-1}], S_{rz} is root zone water content [mm], and $SR_{\max}$ is maximum root zone water content [mm]. $g_{s\max}$ is a prescribed constant based on LULC type. S_{rz} is a prognostic variable calculated in the runoff component, and $SR_{\max}$ is a prescribed constant based on soil type.

3.1.3 Irrigation for paddy fields

Most of the agricultural land in the basin is dry land, and paddy fields occupy less than 10% of total agricultural lands, which means that less than 4% of the basin is paddy fields. However, water needed for growing rice is significantly higher than that needed for dry land fields. Thus, since irrigation for paddy fields might have a significant impact on the hydrological cycle of the basin, an irrigation scheme for paddy fields was incorporated in the model. Though actual water management by farmers varies with each farmer, we adopted one presumably standard water management scheme in the region based on interviews with farmers. River water and groundwater are two main sources of irrigation water in the agricultural area of the basin, and the farmer can select which to use. At the beginning of the irrigation period, 10 mm water is first provided to the paddies. During the normal period of the growing season, losses from evapotranspiration and infiltration are compensated by irrigation to maintain the water level of each plot at 10 mm. The levee height of the plot is uniformly set at 30 cm. When the ponding depth of the paddy lot exceeds the prescribed levee height, excess water overflows. All of the overflowed water is considered to contribute to river flow directly without any retarding process by ponding in canals.

3.1.4 Runoff

The basic concept of the TOP-Runoff module is based on TOPMODEL (Beven & Kirkby, 1979). Though the TOPMODEL concept was originally derived from small-scale catchments, the same concept is now used in global-scale land surface models (LSM) such as MATSIRO (Takata, 2003), which is coupled with an atmospheric general circulation model developed at the Center for Climate System Research, the University of Tokyo, and the National Institute for Environmental Studies, CCSR/NIES AGCM (Numaguti *et al*., 1997). While many variations of the original version of TOPMODEL have been developed, the basic TOPMODEL concept is adopted in our model.

3.1.5 River runoff routing

Calculated runoff and dissolved iron flux are routed along the river network. The TRIP data set for LSM as a GCM component (Oki & Sud, 1998) was used as the river network. Since some part of the TRIP data set did not follow the actual river course, the data set was modified according to another detailed river network data set, which was constructed based on topographical maps (Yermoshin *et al*., 2007). In the schematic diagram of the hydrological model shown in Fig. 3, the river network of the basin is also shown. River runoff velocity is one of the calibration variables, and prescribed as a constant value. In addition, a river meandering coefficient was prescribed with a constant value of 1.4.

We did not consider the freezing of river water. In reality, the major part of the river water in the Amur River basin is partly frozen during the period from the end of November to the middle of April. However, requiring a precise prediction of the discharge during the period of river water freezing is not important from the viewpoint of assessing the total amount of dissolved iron, since the total amount of dissolved iron during the freezing season is much less than that during the non-freezing season.

3.2 Data and parameter setting

An NCEP2 data set with a spatial resolution of about 2.0°×2.0° was utilized as climate forcing data. These data included short wave radiation, long wave radiation, specific humidity, wind speed, and air temperature. The daily precipitation rate was obtained from the APHRODITE dataset (Yatagai *et al*., 2009) at a spatial resolution of 0.5°×0.5°.

As for the validation of the results of the hydrological model, river discharge was utilized. The observation points for river discharge are shown in Fig. 1. We obtained observed discharge data from the main course (stations 1, 2, 8, 9, 10) and at several large tributaries (stations 3-7). The discharge data were provided by the Federal Service for Hydrometeorology and Environmental Monitoring (ROSHYDROMET) and the Global Runoff Data Center (GRDC) in Koblenz, Germany <http://grdc.bafg.de>. The time resolution was daily at stations 8 to 10, and monthly at other stations.

Spatially distributed data are LULC, soil properties and DEM. Since the LULC map shown in Fig. 2 was originally in a vector format, the data were converted to a raster format with spatial resolution of 1,000 m. SRTM3 data derived from the Shuttle Radar Topography Mission of NASA were used for DEM. A coarser DEM data set with a grid size of 1,000 m was produced by averaging SRTM3 for the analysis. Soil properties such as hydraulic conductivity, and field capacity were obtained from the ISLSCP2 data set (Hall *et al*., 2005) with a spatial resolution of 0.5º. According to these spatially distributed data, parameters needed to run the model were assigned.

4. Results and Discussion

4.1 Comparison of spatial distribution of precipitation

We compared the spatial distribution of average annual precipitation during the period from 1981 to 1990 between NCEP2 data and APHRODITE data. The results are shown in Fig. 4. NCEP2 data were interpolated to match the spatial resolution of the APHRODITE data set.The results show clearly that the NCEP2 data set gives a significantly larger amount of precipitation compared with APHRODITE. The aerial average value from NCEP2 data and APHRODITE data is 701mm and 535mm, respectively. Figure 4 also shows the spatial distribution of precipitation amount differences between the two data sets. Within most of the eastern part of the basin, the precipitation amount of the NCEP2 data is larger than that of the APHRODITE data. Though it is very difficult to acquire a reliable actual precipitation data set, we can refer to one figure from Simonov and Dahmer (2008) as a reference of the actual precipitation distribution in the basin, shown with a red line in Fig. 1. Compared with Fig. 4, the spatial distribution pattern and absolute value from the APHRODITE data seem more similar to Fig. 1. This suggests that the APHRODITE data could have a potential to improve the results of hydrological simulation.

4.2 Simulation results

Figure 5 shows the calculated discharges by using two different precipitation data sets (NCEP2 and APHRODITE) and observed discharges along the main course and several tributaries of the Amur River. Though no parameter calibration was executed, we obtained a fairly good result when we used the APHRODITE precipitation dataset. In contrast, when we used the NCEP2 precipitation dataset, the obtained discharges were significantly overestimated at most points. Especially at observation stations 8 to 10, calculated discharges using the NCEP2 dataset were almost double the observed discharges in the annual base. On the other hand, the differences between the observed and calculated discharge at observation points 1 and 2 were comparably small. This overall trend of calculated discharge differences coincides with the spatial pattern

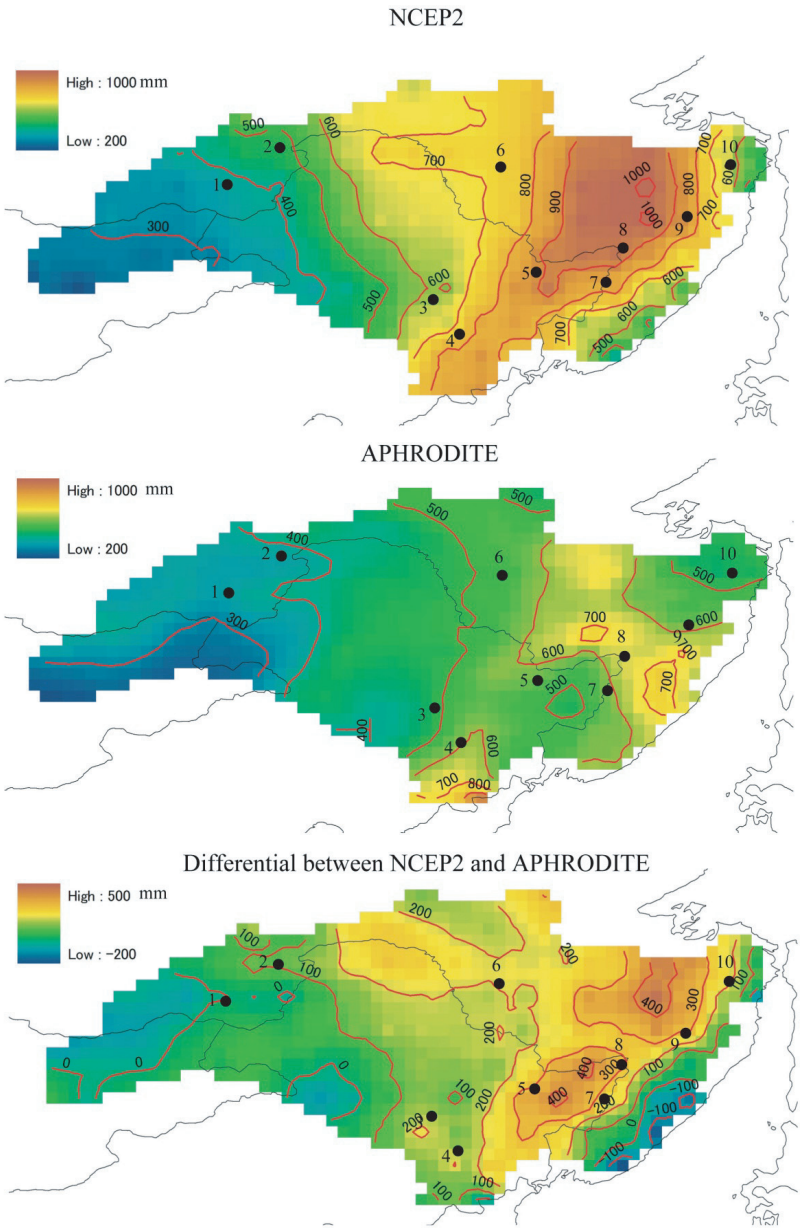

Fig. 4 Comparison of spatial distribution patterns of average annual precipitation between NCEP2 data and APHRODITE data. The period averaged is from 1981 to 1990. Discharge observation stations are also indicated by black-filled circles in each figure.

difference between NCEP2 and APHRODITE; *i.e.*, the spatial pattern of discrepancy between the NCEP2 and APHRODITE data sets is largest in the middle to lower part of the basin and smallest in the upper part of the basin as shown in the bottom figure of Fig. 5. This indicates that the NCEP2 data set might give an overestimation of precipitation, especially in the middle to lower parts of the Amur River basin. Our results are also consistent with the results of Betts *et al*. (2006), whose study showed that the NCEP2 precipitation of this region is much higher than the Global Precipitation Climatology Project (GPCP) data set.

We evaluated the accuracy of each simulated result using Nash and Sutcliffe (1970) criteria (Table 2). Since a Nash and Sutcliffe criteria value larger than 0.5 means moderately good or good agreement with observed values, it can be said that the results simulated using APHRODITE data give relatively good results compared with those using the NCEP2 data set. Of course, after executing parameter calibrations, the results calculated using NCEP2 reanalysis can also give good agreement with observed data. The calibrated parameter sets, however, were not within the physically valid ranges of each parameter. Thus, considering that calculated discharge data can be a gross hydrological index of a basin, we can conclude that the APHRODITE precipitation dataset is more accurate than the NCEP2 dataset, especially in the Amur River basin. It has also been proven that APHRODITE can give better results in discharge simulation of the Amur River basin.

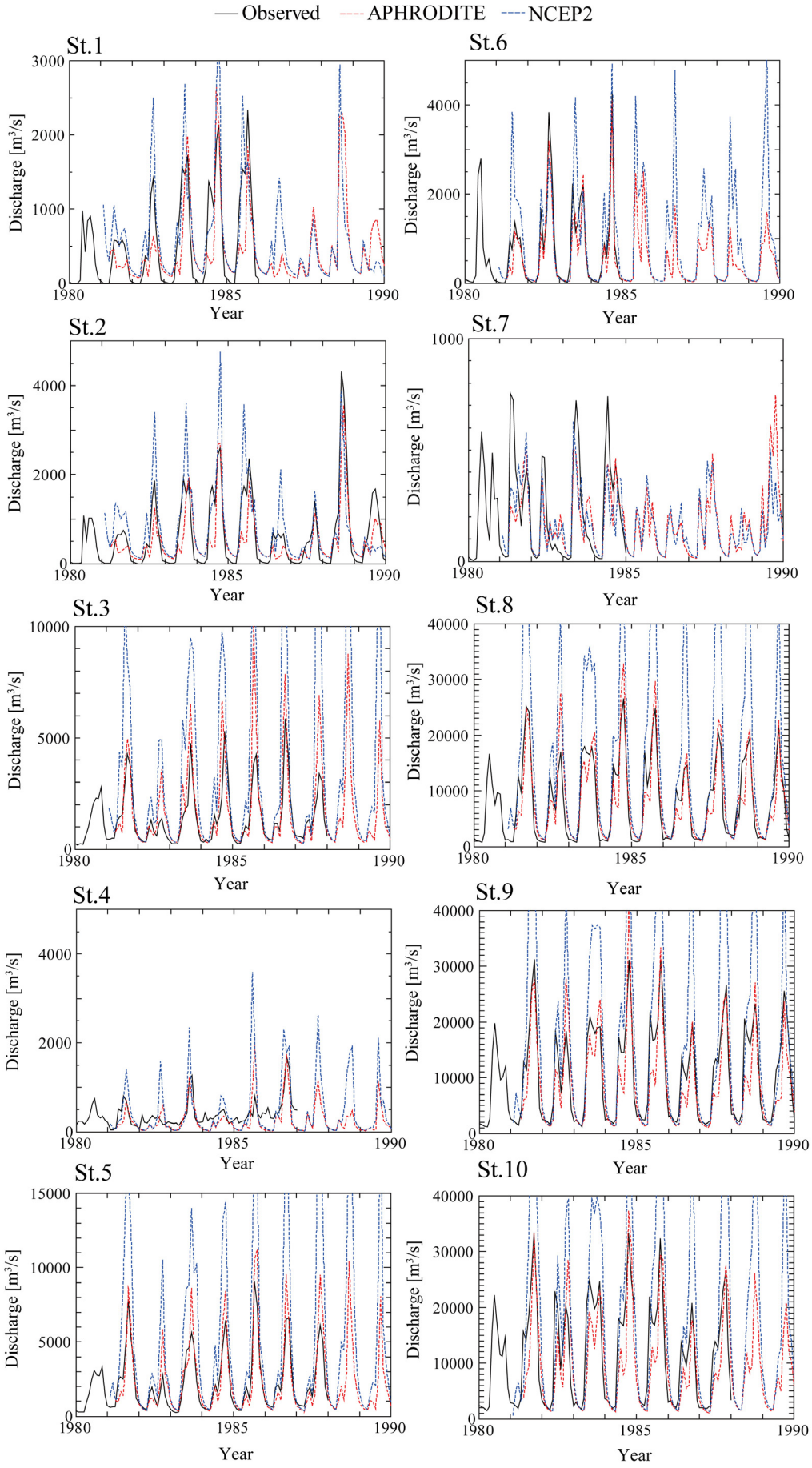

Fig. 5 Comparison of discharge calculated by using NCEP2 data and that by using APHRODITE data.

Table 2 Values of Nash-Sutcliffe criteria at each observation point.

Station	APHRODITE	NCEP2	Catchment area ($\times 10^3 km^2$)
1	0.5	0.5	175
2	0.7	0.4	200
3	0.2	–7.5	391
4	0.1	–2.4	44
5	0.7	–4.9	400
6	0.9	0.4	67
7	0.5	0.5	24
8	0.8	–1.8	1,600
9	0.7	–1.1	1,730
10	0.6	–1.2	1,790

5. Conclusion

We constructed a hydrological model of the Amur River basin to evaluate dissolved iron production amounts. Since the accuracy of hydrological models is significantly related to precipitation input, results simulated using two different precipitation data sets were examined. For precipitation data, NCEP2 and APHRODITE were used. We confirmed that the NCEP2 dataset might give overestimated precipitation, especially in the middle to lower part of the Amur River basin. It was also suggested that APHRODITE data have a potential to give better results compared with NCEP2 data for the Amur River basin.

Acknowledgments

This work was undertaken under the framework of an international project entitled 'Human activities in Northeastern Asia and their impact on the biological productivity of the North Pacific Ocean' funded by the Research Institute for Humanity and Nature (RIHN) during the period from 2005 to 2009. The authors express their thanks to Global Soil Data Task, the IGBP, ORNL DAAC and ISLSCP Initiative II for providing soil characteristic data. We deeply thank all the staff in ROSHYDROMET, and in particular G. Alexander for his special collaboration in this work.

References

Betts, A.K., M. Zhao, P.A. Dirmeyer and A.C.M. Beljaars (2006) Comparison of ERA40 and NCEP/DOE near-surface data sets with other ISLSCP-II data sets. *Journal of Geophysical Research*, Vol. 111, D22S04, doi:10.1029/2006JD007174.

Beven, K.J. and M.J. Kirkby (1979) A physically based, variable contributing area model of basin hydrology. *Hydrological Science Bulletin*, 24: 43-69.

Boyd, P.W., C.S. Law, C.S. Wong, Y. Nojiri *et al*. (2004) The decline and fate of an iron-induced subarctic plankton bloom. *Nature*, 428: 549-553.

DeWalle, D.R. and A. Rango (2008) *Principles of Snow Hydrology*, Cambridge University Press, New York.

Ducklow, H.W., J.L. Oliver and W.O. Smith, Jr. (2003) The role of iron as a limiting nutrient for marine plankton processes. *In*: J.M. Melillo, C.B. Field and B. Moldan, eds., *Interactions of the Major Biogeochemical Cycles: Global Change And Human Impacts*, 295-310, Island Press, Washington.

Global Soil Data Task (2000) Global Soil Data Products CD-ROM (IGBP-DIS). International Geosphere-Biosphere Programme, Data and Information System, Potsdam, Germany. Available from Oak Ridge National Laboratory Distributed Active Archive Center, Oak Ridge, Tennessee, U.S.A.

Hall, Forrest G., G. Collatz, S. Los, E. Brown de Colstoun and D. Landis, eds. (2005) ISLSCP Initiative II. NASA. DVD/CD-ROM. NASA.

Hirabayashi, Y., S. Kanae, K. Motoya, K. Masuda and P. Doll (2008) A 59-year (1948-2006) global meteorological forcing data set for land surface models. Part 1: Development of daily forcing and assessment of precipitation intensity. *Hydrological Research Letters*, 2: 65-69.

Hock, R. (2003) Temperature index melt modelling in mountain areas. *Journal of Hydrology*, 282: 104-115.

Kållberg, P., A. Simmons, S. Uppala and M. Fuentes (2004) The ERA-40 archive. ERA-40 Project Report, 17, p.31, European Center For Med.-Range Weather Forecasts, Reading, U. K. <http://www.ecmwf.int/publications/library/ecpublications/_pdf/era40/ERA40_PRS17.pdf>

Kanamitsu, M., W. Ebisuzaki, J. Woollen, S.-K. Yang, J.J. Hnilo, M. Fiorino and G.L. Potter (2002) NCEP-DEO AMIP-II Reanalysis (R-2). *Bulletin of the American Meteorological Society*, 11: 1631-1643.

Kondoh, J. (1994) *Meteorology of Water Environment: Water and Heat Budget at the Surface*, Asakura Press, Tokyo. (in Japanese)

Li, Y., J. Cui, T. Zhang and H. Zhao (2003) Measurement of evapotranspiration of irrigated spring wheat and maize in a semi-arid region of north China. *Agricultural Water Management*, 61: 1-12

Liua, X., J. Jina, S.J. Herbert, Q. Zhanga and G. Wang (2005) Yield components, dry matter, LAI and LAD of soybeans in Northeast China. *Field Crop Research*, 93: 85-93.

Lundberg, A. and S. Halldin (2001) Snow interception evaporation. Review of measurement techniques, processes, models. *Theoretical and Applied Climatology*, 70: 117-133.

Martin, J.H. and S.E. Fitzwater (1988) Iron deficiency limits phytoplankton in the northeast Pacific subarctic. *Nature*, 311: 341-343.

Monteith, J.L. (1965) Evaporation and environment. *In*: The state and movement of water in living organisms. *Proceeding of 19th Symposium of the Society for Experimental Biology, Swansea 1964*, pp.205-234, Academic Press, UK.

Nash J. E. and J.V. Sutcliffe (1970) River flow forecasting through conceptual models 1, A discussion of principles. *Journal of Hydrology,* 10: 282-290.

Numaguti, A., M. Takahashi, T. Nakajima and A. Sumi (1997) Description of CCSR/NIES atmospheric general circulation model. *CGER's Supercomputer Monograph Report*, 3, 1-48.

Ogi, M., Y. Tachibana, F. Nishio and M.A. Danchenkov (2001) Does the fresh water supply from the Amur River flowing into the Sea of Okhotsk affect sea ice formation? *Journal of the Meteorological Society of Japan*, 79: 123-129.

Oki, T. and Y.C. Sud (1998) Design of total runoff integrating pathways (TRIP)−A global river channel network. *Earth Interactions*, 1(2): 1-37.

Park, H., A. Sakashita, Z. Da and K. Yoshida (2001) Paddy development and national farm management in the Sanjiang plain: Case study conducted at the Xinghua farm. *The Review of Agricultural Economics*, 57: 85-98.

Scurlock, J.M.O., G.P. Asner and S.T. Gower (2001) Worldwide historical estimates of leaf area index, 1932-2000. *ORNL Technical Memorandum ORNL/TM-2001/268*, Oak Ridge National Laboratory, Oak Ridge, Tennessee.

Simonov, E.A. and T.D. Dahmer (2008) *Amur-Heilong River Basin Reader*, Ecosystems Ltd., Hong Kong.

Takata, K., S. Emori and T. Watanabe (2003) Development of the

minimal advanced treatments of surface interaction and runoff. *Global and Planetary Change*, 38: 209-222.

Toba, T. and T. Ohta (2005) Observational study of the factors that influence interception loss in boreal and temperate forests. *Journal of Hydrology*, 313: 208-220.

Wang, Z., S. Zhang and Z. Bai (2004) Effects of land use change on values of ecosystem services of Sanjiang Plain, China. *China Environmental Science*, 24(1): 125-128.

Watanabe, T. and J. Kondoh (1990) The influence of canopy structure and density upon the mixing length within and above vegetation. *Journal of the Meteorological Society of Japan*, 68: 227-235.

Watanabe, T. (1994) Bulk parameterization for a vegetated surface and its application to a simulation of nocturnal drainage flow. *Boundary-Layer Meteorology*, 70: 13-35.

Yatagai, A., O. Arakawa, K. Kamiguchi, H. Kawamoto, M.I. Nodzu and A. Hamada (2009) A 44-year daily gridded precipitation dataset for Asia based on a dense network of rain gauges. *SOLA* , 5: 137-140, doi:10.2151/sola.2009-035.

Yermoshin, V.V., S.S. Ganzei, A.V. Murzin, N.V. Mishina and E.P. Kudryavtzeva (2007) Creation of GIS for Amur River basin: the basic geographical information. *Annual Report on Amur-Okhotsk Project,* No.4, 151-159.

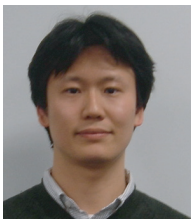

Takeo ONISHI

Takeo ONISHI is an Assistant Professor of the Faculty of Applied Biological Sciences, Gifu University. He received his Doctorate in Agriculture at Kyoto University (2004). His current interests are hydrological modeling, interactions between hydrological cycles and biogeochemical cycles on terrestrial area and hydrological interactions between land and ocean. His research works place especial emphasis on the evaluation of anthropogenic impacts such as agriculture, forestry and fisheries on hydrological and biogeochemical cycles.

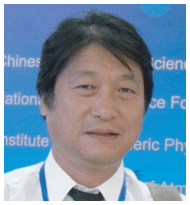

Muneoki YOH

Dr. Muneoki YOH works in the Division of Environmental Science on Biosphere, Institute of Agriculture, Tokyo University of Agriculture and Technology (Fuchu, Tokyo, Japan). He got his doctorate in science from Nagoya University in 1991 with a dissertation study on the biogeochemical behavior of N_2O in freshwater lakes. His major interest has been biogeochemistry, mainly regarding nitrogen, but recently extending to the cycling of other elements such as carbon and iron. His present fieldwork includes lake, stream, river, wetland, agricultural field, forest and alpine ecosystems. His recent typical subjects include 1) nitrogen saturation and acidification in forest ecosystems in China and Japan and 2) dissolved iron in terrestrial environments.

Seiya NAGAO

Seiya NAGAO is a Professor at the Low Level Radioactivity Laboratory, Institute of Nature and Environmental Technology, Kanazawa University. His current interests are 1) biogeochemistry of dissolved and particulate organic matter and iron in river watershed systems including coastal marine environments, 2) migration behavior and its characteristics and the functionality of dissolved organic matter such as humic substances in groundwater, 3) transport processes of radiocesium in river, lake and marine environments. His research work uses radioisotopes and stable isotopic ratios as tracers of organic matter and suspended solids. He also uses spectroscopic and chromatographic techniques to characterize dissolved organic matter in natural waters.

Hideaki SHIBATA

Hideaki SHIBATA is a Professor at the Field Science Center for Northern Biosphere, Hokkaido University. His current interests are forest biogeochemistry, ecosystem ecology, hydrology and soil science with the impact of human activities (such as atmospheric deposition, climate change, land-use and land-cover changes) in mainly forest ecosystems. At present, his principal projects focus on (1) nitrogen and carbon cycling and stream chemistry in forest watersheds, (2) effects of natural and anthropogenic disturbances on ecosystem processes and services in forest landscapes and (3) the role of *sasa* dwarf bamboo on carbon and nitrogen cycling in forest ecosystems.

(Received 27 September 2011, Accepted 26 December 2011)